Molecular Cell
Article

Synthesis of Empty Bacterial Microcompartments, Directed Organelle Protein Incorporation, and Evidence of Filament-Associated Organelle Movement

Joshua B. Parsons,[1,5] Stefanie Frank,[1,5] David Bhella,[2] Mingzhi Liang,[3] Michael B. Prentice,[3,4] Daniel P. Mulvihill,[1] and Martin J. Warren[1,*]
[1]Centre for Molecular Processing, Department of Biosciences, University of Kent, Canterbury, Kent CT2 7NJ, UK
[2]MRC Virology Unit, University of Glasgow, Glasgow G11 5JR, Scotland
[3]Department of Microbiology
[4]Department of Pathology
University College Cork, Cork, Ireland
[5]These authors contributed equally to this work
*Correspondence: m.j.warren@kent.ac.uk
DOI 10.1016/j.molcel.2010.04.008

SUMMARY

Compartmentalization is an important process, since it allows the segregation of metabolic activities and, in the era of synthetic biology, represents an important tool by which defined microenvironments can be created for specific metabolic functions. Indeed, some bacteria make specialized proteinaceous metabolic compartments called bacterial microcompartments (BMCs) or metabolosomes. Here we demonstrate that the shell of the metabolosome (representing an empty BMC) can be produced within *E. coli* cells by the coordinated expression of genes encoding structural proteins. A plethora of diverse structures can be generated by changing the expression profile of these genes, including the formation of large axial filaments that interfere with septation. Fusing GFP to PduC, PduD, or PduV, none of which are shell proteins, allows regiospecific targeting of the reporter group to the empty BMC. Live cell imaging provides unexpected evidence of filament-associated BMC movement within the cell in the presence of PduV.

INTRODUCTION

Organelles, one of the defining characteristics of the eukaryotic cell, are structures that are used to compartmentalize metabolic activities and segregate genetic information and its transfer. Such detachment allows for enhanced organization and greater regulation of energy and metabolic requirements. Intriguingly, though, the appearance of separate physical compartments is not restricted to eukaryotes. Some bacteria are able to form internal partitions called bacterial microcompartments (BMCs), which are metabolically active structures that are bound by a proteinaceous shell and located within the cellular cytoplasm (Cheng et al., 2008; Tanaka et al., 2008; Yeates et al., 2008). From an investigative point of view, BMCs are of interest since their appearance draws parallels with eukaryotic organelles, the development of cellular strategies to cope with metabolic stress, and the construction of supramolecular complexes to improve substrate channeling.

The best-known example of the BMC is the carboxysome, a polyhedral edifice found in cyanobacteria and some chemoautotrophic bacteria that is associated with the fixation of carbon dioxide (Iancu et al., 2007; Schmid et al., 2006; Tanaka et al., 2008). The carboxysome has a highly organized composition that is about 100 nm in diameter and houses both the Calvin cycle enzyme ribulose-1,5-bisphosphate carboxylase/oxygenase (RuBisCO) and carbonic anhydrase. The ability to catalyze the rapid interconversion of carbon dioxide and bicarbonate inside the microcompartment is thought to concentrate carbon dioxide and overcome the well-documented inefficiency of RuBisCO.

The current model of the carboxysome predicts that organized arrangements of the enzymes RuBisCo and carbonic anhydrase are contained within a quasi-icosahedral structure encased by outer shell proteins (Iancu et al., 2007; Schmid et al., 2006; Tanaka et al., 2008). The precise mechanism of assembly of the shell and the way in which enzymes are targeted to its interior are not known. There are at least three proteins that make up the facets of the shell in the α-type carboxysome (CsoS1A-C) and five in the β-type carboxysome (CcmK1-4 and CcmO) (Beeby et al., 2009; Tanaka et al., 2008; Yeates et al., 2008). The structures of some of these proteins have been determined and have been shown to form hexameric units that self-assemble into sheets to generate the facets of the icosahedral microcompartment (Kerfeld et al., 2005). The vertices of the complex are formed by a protein that forms a pentameric structure (CsoS4A and CcmL in the α- and β-type carboxysome, respectively), which combines with the hexameric structures to generate curvature to allow closure of the outer casing of the assembly (Tanaka et al., 2008).

However, many other bacteria also have the ability to make related carboxysome-like structures but which house different

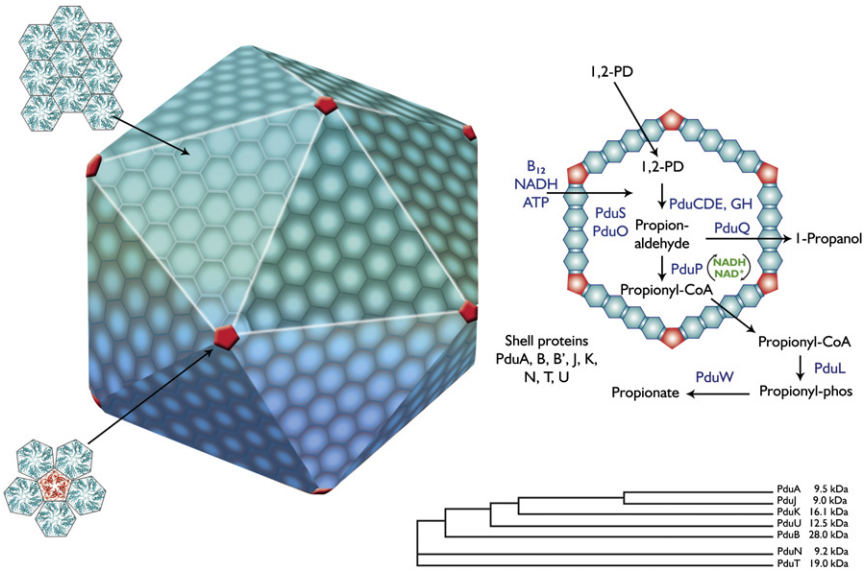

Figure 1. The Bacterial Microcompartment and the Associated Shell Proteins

BMCs are proteinaceous structures that form polyhedral shapes within the prokaryotic cell. The faces of the structure are formed from the association of hexagonal shell proteins, the most abundant of which in the propanediol metabolosome are PduA, PduB, and PduJ. The vertex of the assembly is formed with a pentameric shell protein, which in the propanediol metabolosome is thought to be PduN (highlighted in red). The metabolism associated with 1,2-propanediol (1,2-PD) is shown schematically. In the propanediol metabolosome, the shell of the structure is thought to be composed from eight shell proteins, although two of three proteins (PduB and PduB′) are synthesized from the same gene but using a slightly different translation start site on the mRNA. These shell proteins all have a degree of sequence similarity, indicating a common evolutionary origin, and this relationship is shown in the form of a cladogram.

metabolic activities (Cheng et al., 2008). The best-characterized of these are the microcompartments associated with ethanolamine (*eut*) and propanediol (*pdu*) utilization (Bobik et al., 1999; Kofoid et al., 1999). Both of these metabolic activities depend on enzymes that require adenosylcobalamin as a coenzyme. As these microcompartments are associated with a specific metabolic activity, they have been termed metabolosomes (Brinsmade et al., 2005). It has been suggested that both propanediol and ethanolamine utilization are contained within microcompartments because of the need to protect the cell from the toxicity of the reactive aldehyde intermediate that is formed during their catabolism (Rondon et al., 1995; Sampson and Bobik, 2008).

The propanediol utilization metabolosome appears both biochemically and structurally to be more complex than the carboxysome. It houses the enzymes responsible for the conversion of 1,2-propanediol into propionaldehyde (the diol dehydratase, which is composed of PduC-D-E) and its disproportionation into 1-propanol (aldehyde dehydrogenase PduQ) and propionyl-CoA (CoA transferase PduP). It also contains the reactivation factors for the diol dehydratase, PduG-H, and enzymes required for the formation of the coenzyme form of cobalamin, PduO and -S. For the construction of the organelle, the *pdu* operon encodes for seven proteins that display sequence similarity to the shell proteins of the carboxysome, including PduA, -B, -J, -K, -N, -T, and -U. Of these it is known that PduB is synthesized in two forms that differ in size by 37 amino acid residues due to two translation start sites on the polycistronic message (Parsons et al., 2008). The two variants are referred to as PduB (28 kDa) and PduB′ (24 kDa) (Havemann and Bobik, 2003; Parsons et al., 2008). By analogy with the carboxysome shell proteins, most of the *pdu* BCM-containing homologs are thought to form hexameric building blocks that pack into protein sheets and comprise the facets of the microcompartment structure (Figure 1). Indeed, recent structural data have confirmed that PduU does form such a hexameric arrangement (Crowley et al., 2008). The vertices of the assemblage are thought to be generated from pentameric forms of PduN (Figure 1), which displays similarity to the pentameric component of the carboxysome CcmL (Tanaka et al., 2008), or possibly from an asymmetric hexamer arrangement, as recently demonstrated for EutS (Tanaka et al., 2010).

Recently, we engineered propanediol utilization activity into a laboratory K12 strain of *E. coli*, an organism that does not possess this ability (Parsons et al., 2008). By cloning the 21 gene *pdu* operon from *Citrobacter freundii* into *E. coli*, we demonstrated that the transformed bacteria become endowed with the ability not only to produce the required diol dehydratase activity but also to construct fully formed and functional metabolosomes. By upregulating the production of individual shell proteins within this strain, it was found that the shape of the microcompartment could be drastically altered (Parsons et al., 2008). Not only did this suggest that these proteins are essential constituents of the shell of the structure, it also demonstrated that the relative proportions of the shell components are important for assembly of these macromolecular structures. However, still, little is known about the biogenesis of the BMCs, for instance whether the shell forms around a predefined scaffold on encased enzymes, which shell proteins interact, how proteins are targeted to the organelle, or how the organelles are distributed intracellularly. In this present research these important issues are addressed.

RESULTS

Cloning of All *pdu* BMC Genes Generates Empty Microcompartments

The *pdu* operon encodes seven shell proteins (PduA, -B, -J, -K, -N, -T, and -U) and one variant (PduB′), which all display similarity to the BMC shell proteins of the carboxysome. Thus, in total, eight proteins appear to be associated with the shell of the propanediol utilization microcompartment. The phylogenetic relationship between the different proteins is shown in Figure 1. Most of the shell proteins have a molecular mass of 9–14 kDa,

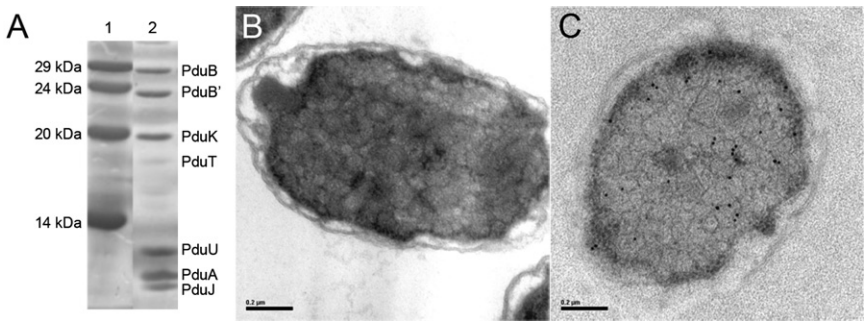

Figure 2. Synthesis of Bacterial Microcompartments by Expression of *pduA-B-J-K-N-U-T*

(A) SDS-PAGE of protein extract from strain expressing *pduA-B-J-K-N-U-T* after sucrose gradient ultracentrifugation (lane 2) in comparison to molecular mass standards (lane 1). The major bands in lane 2 were extracted, digested, and analyzed by MALDI to confirm their identity as shown.

(B) Thin section of *E. coli* cell expressing *pduA-B-J-K-N-U-T* as viewed by TEM. The cytoplasm of the cell is seen to be full of bodies with delimiting boundaries, indicating the presence of BMCs.

(C) Thin section of *E. coli* cell expressing *pduA-B-J-K-N-U-T* but cross-reacted with anti-PduA antibodies and then with a secondary antibody conjugated to 15 nm gold particles. The gold particles are seen to localize at the boundaries of the structures, consistent with PduA acting as a shell protein.

but a number (PduB, PduB′, and PduT) are more than twice this size and appear to have arisen by gene duplication and fusion, since they contain a tandem repeat of the BMC motif.

In an attempt to produce an empty metabolosome, it was decided to clone just the genes encoding the predicted shell proteins into a suitable vector. A description of all the strains and plasmids used in this study is given in Table S1 available online. The genes were cloned in the same order as exists in the wild-type *pdu* operon, except for *pduU* and *pduT*, whose order was reversed for practical cloning reasons, omitting any intervening nonshell protein genes. By using technology developed for recombinant production of complex metabolic pathways, the genes encoding the *pdu* BMC proteins (*pduA*, *-B*, *-J*, *-K*, *-N*, *-T*, and *-U*) were linked and locked into position within a pET vector (McGoldrick et al., 2005). After transformation of this plasmid into *E. coli* BL21 cells, the resultant strain was grown, induced with IPTG, and incubated overnight. The cells were subsequently analyzed for the production of recombinant proteins by SDS-PAGE and the appearance of microcompartments by thin sectioning and electron microscopy.

An analysis of the protein profile of a crude cell lysate of the *E. coli* strain containing *pduA-B-J-K-N-U-T* revealed the presence of overproduced protein bands that corresponded to the predicted molecular mass of the encoded gene products. Moreover, the proteins appeared to form a large macromolecular complex, as they could be separated from the rest of the soluble cytoplasmic proteins by ultracentrifugation on a sucrose gradient (Figure 2A). Although not completely homogeneous, the pellet from the ultracentrifugation was found to contain enhanced levels of PduA, -B, -B′, -J, -K, -U, and -T by SDS-PAGE. The identities of the protein bands were confirmed by MALDI analysis after the protein bands had been extracted and subjected to proteolysis by trypsin. PduN was not detectable in this profile, but as it is suspected to act as a vertex protein, it is likely to be present in only very small quantities.

Thin sectioning and negative staining of bacteria harboring the plasmid containing *pduA-B-J-K-N-U-T* revealed the presence of internal cytoplasmic bodies with delimiting boundaries (Figure 2B) of similar size (about 100 nm diameter) to recombinant metabolosomes observed when the whole *pdu* operon is expressed in *E. coli* (Parsons et al., 2008). The cytoplasm of the bacteria expressing *pduA-B-J-K-N-U-T* was seen to be full of the microcompartments with other cytoplasmic components such as ribosomes displaced to the side. To determine whether the structures are associated with the shell proteins, thin sections of bacteria containing the recombinant microcompartments were cross-reacted with an antibody raised against PduA. This was subsequently detected with a secondary antibody conjugated to 15 nm gold particles. The resulting image revealed that the majority of the gold particles were localized to the boundaries of the microcompartments (Figure 2C). It would thus appear that these structural enclosures, resembling metabolosomes but with no propanediol utilization activity, can be formed by the coordinated production of all the propanediol utilization shell proteins. This indicates that no further ancillary factors encoded within the *pdu* operon are required for the actual assembly of the microcompartment and that the shell of the BMC does not have to be formed around a scaffold of enzyme complexes such as the 1,2-propanediol dehydratase (PduC-D-E).

PduT and PduU Are Not Essential for BMC Formation

Next we sought to remove a number of the shell proteins from the artificial construct to determine the minimum number of shell proteins required for assembly of the microcompartment. Constructs containing *pduA-B-J-K-N-U* and *pduA-B-J-K-N*, when transformed into *E. coli*, were also able to form delimited structures within the cell cytoplasm (Figures 3A and 3B). This was deduced from thin sections of the appropriate recombinant *E. coli* strains when viewed by TEM. In both strains, the proteins corresponding to the cloned genes could be visualized on SDS gels when crude cell extracts were analyzed (data not shown). Moreover, the BMC-containing proteins from these strains could be purified by sucrose gradient ultracentrifugation, indicating that large macromolecular complexes were being formed. Thus, it would appear that PduU and PduT are not essential for organelle biogenesis. The structure of PduU has recently been reported, and although its topology clearly confirms it as a member of the BMC family (Crowley et al., 2008), it appears that deletion of *pduU* from the *S. enterica* operon does not prevent metabolosome formation. PduT is a specialized metalloprotein that contains an Fe-S center (Parsons et al., 2008). The role for this redox group has not yet been established.

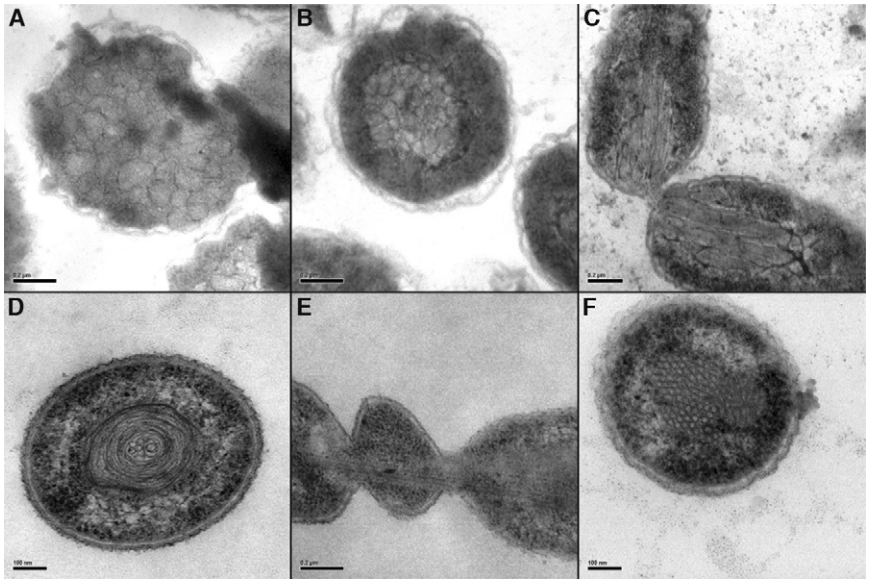

Figure 3. Effect of Combinations of PduA-B-J-K-N-U on Organelle Formation

(A) Thin section of *E. coli* cell expressing *pduA-B-J-K-N-U*. The cells form BMCs with clear boundaries.

(B) Thin section of *E. coli* cell expressing *pduA-B-J-K-N*. The cells form BMCs with clear boundaries.

(C) Thin section of *E. coli* cell expressing *pduA-B-J-K*. The cells form elongated structures but do not appear to have clear boundaries. The fibrous structures appear to interfere with septation.

(D) Thin section of *E. coli* cell expressing *pduA-B-J*. The cells appear to form a protein sheet that is rolled up.

(E) Thin section of *E. coli* cell expressing *pduA-B*. The cells form elongated filamentous structures. The fibrous structures appear to interfere with septation and cell division.

(F) Thin section of *E. coli* cell expressing *pduA*. The protein appears to form a lattice-like structure, giving a hexagonal arrangement. See also Figure S1.

PduJ, PduK, and PduN Are Essential for BMC Formation

A further reduction in the number of genes within the original artificial shell construct did prevent microcompartment formation. Thus, a strain harboring *pduA-B-J-K*, when viewed by TEM after thin sectioning, revealed structures that appear to consist of small rectangular arrangements that are linked together to give extensive assemblies. These structures are very long and fibrous and at times appear to interfere with cell division by preventing septation (Figure 3C). They are quite distinct from the microcompartments formed in the presence of PduN. From this it can be concluded that PduN is essential for microcompartment formation, consistent with the view that the protein forms the vertices of the structure.

Similarly, constructs containing *pduA-B-J-N*, *pduA-B-K-N*, and *pduB-J-K-N* also failed to generate BMC-like structures when induced in appropriate *E. coli* strains (Figure S1). It would therefore appear that PduA, PduJ, PduK, and PduN play essential roles in the formation of the microcompartment.

Protein Sheets and Filaments in *E. coli*

An *E. coli* strain containing *pduA-B-J* produced further unusual structures (Figure 3D). Elongated laminar fibers were observed, which on cross-section gave a spiral appearance. It seems as though these proteins form a sheet that folds to give a Swiss roll type of structure. The lack of PduK and PduN clearly affects the ability of these protein complexes to form enclosed compartments. Interestingly, when the protein profile of this strain was analyzed by SDS-PAGE, no protein bands corresponding to PduA, -B, and -J were detected (data not shown). Thus, although the presence of PduA, -B, and -J gives rise to large cellular molecular formations, the proteins must polymerize to generate a complex that does not run into the polyacrylamide gel.

When *pduA-B* was transformed into *E. coli*, similar sheet- and fiber-like structures were observed, which also appear to interfere with cell division (Figure 3E). PduA and PduB must interact, since they could be copurified from cleared cell lysates by ultracentrifugation and visualized on stained SDS gels (data not shown).

Finally, overproduction of PduA alone in *E. coli* gave an altogether different structure, forming a lattice of cytoplasmic axial filaments. Longitudinal sections revealed the appearance of very regular fibers, giving a laminar appearance. On cross-section the cells appeared to form a hexagonal lattice, which in some cells took up the majority of the cellular cytoplasm. PduA appears to form a crystalline structure within the cytoplasm of the cell (Figure 3F).

A variant of PduA, termed PduA*, was generated serendipitously by a frameshift in the gene, whereby the final four bases at the 3′ terminus of the gene were removed allowing the fusion of the noncoding DNA from the vector to become incorporated into the open reading frame. This resulted in the exchange of the terminal amino acid of the protein and the addition of a further 23 amino acids to the C terminus of the protein (see the Supplemental Information for details). This form of the protein was significantly more soluble and resulted in the dramatic appearance of appreciably more hexagon-like arrays in cells producing the PduA* (Figure 4A). Evidence that PduA* formed large aggregates came from ultracentrifugation studies of the cytoplasmic extract of the strain. Here, after cell lysis and centrifugation to cell debris and membranes, the pellet obtained from ultracentrifugation was found to contain PduA*. To confirm that the laminar and hexameric structures observed in the bacterial thin sections were derived from the overproduction of PduA*, the thin sections were cross-reacted with a PduA antibody and then with a secondary gold-particle-linked antibody. Gold particles were observed only with the filamentous structures seen in the thin sections (Figures 4B and 4C).

Electron tomography of resin-embedded cell sections provides a three-dimensional view of the laminar and hexagonally packed structures formed by expression of PduA* in *E. coli* (Figures 4D–4H and). Transverse sections viewed in three-dimensions reveal that the hexagonally packed circular structures

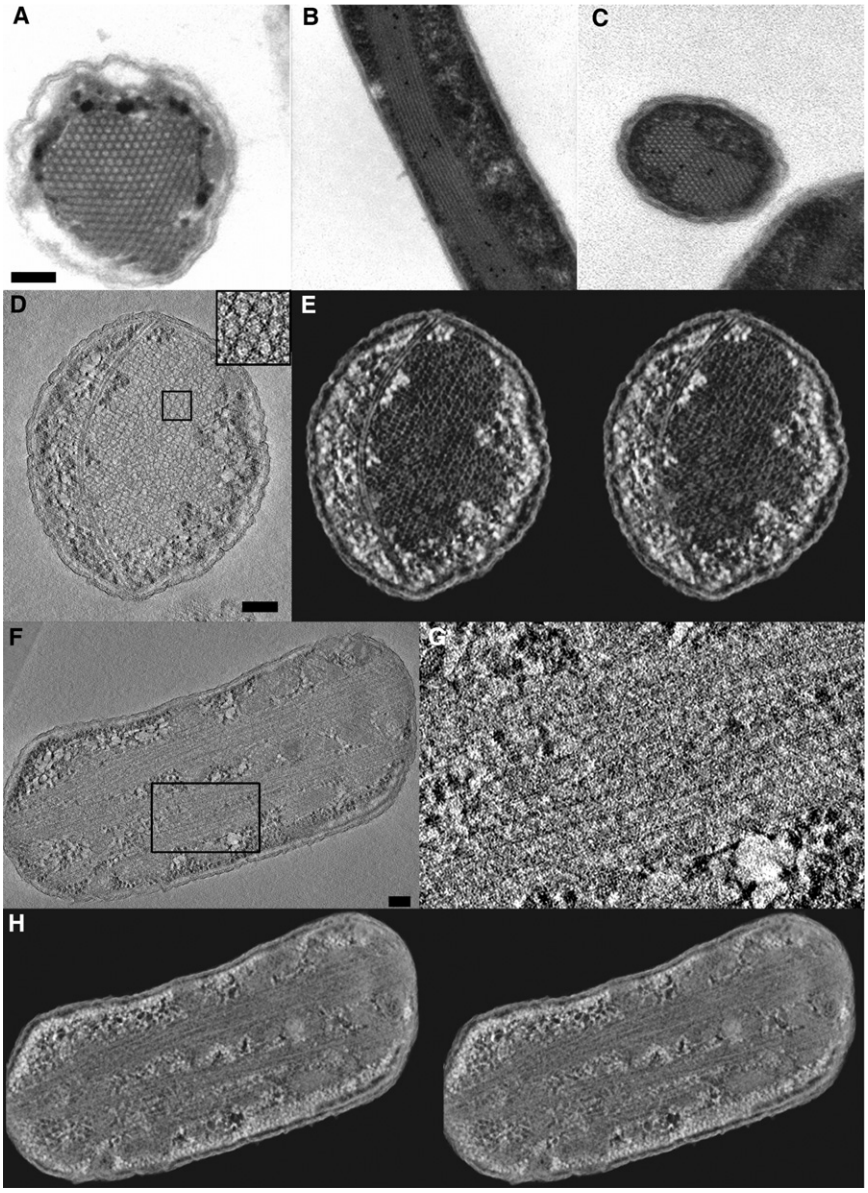

Figure 4. Analysis of Cells Overproducing PduA*, a More Soluble Form of PduA

(A) Section of *E. coli* overproducing PduA*, giving rise to a hexagonal lattice.

(B) Longitudinal section of *E. coli* overproducing PduA*, but this time cross-reacted with anti-PduA antibodies and then with a secondary antibody conjugated to 15 nm gold particles. The gold particles are only associated with the protein filaments that are observed in the cell.

(C) Section as in (A) above, but this time cross-reacted with anti-PduA antibodies and then with a secondary antibody conjugated to 15 nm gold particles. The gold particles are largely associated with the protein filaments that are observed in the cell.

(D) Slice (20 nm) through the z axis in a transverse section tomogram of *pduA** expressing *E. coli* showing hexagonally packed structures (inset); scale bar, 100 nm. Volume rendering of this reconstruction reveals that these structures are filamentous.

(E) Stereo view (also see Movie S1).

(F–H) Longitudinal sections reveal that the laminar structures are also filamentous and show features consistent with helical symmetry (and Movie S2).

appear filamentous, while longitudinal sections indicate that the laminar structures are also packed filaments. Close inspection of the filaments reveals striated patterns (Figure 4G), while power spectra of these regions show layer lines, suggesting a helical structure (data not shown).

PduA Interacts with PduB, PduJ, PduK, and PduU

The difference in the appearance of the cellular structures seen with PduA overproduction and that of PduA and PduB joint overproduction suggested an interaction between these two components. This was confirmed by experiments in which PduA was N-terminally His tagged and coproduced in vivo with PduB. When the cell extract was passed over a nickel affinity column, both PduB and PduB′ were found to elute with PduA in the presence of high levels of imidazole. Control experiments demonstrated that PduB and PduB′ do not bind to the nickel column in the absence of bound PduA.

This series of experiments was extended to detect any other interactions with the remaining shell proteins encoded within the pdu operon as well as the proteins of unknown function, PduM and PduV. The His-tagged PduA bait was coproduced with these individual untagged products. The experiment was then redone using His-tagged PduB, His-tagged PduJ, and His-tagged PduK as bait. The results are summarized in Table 1. It was found that PduA interacted with PduJ, PduK, PduN, and PduU. Control experiments revealed that the untagged protein did not interact with the nickel columns themselves, indicating the interaction with PduA was specific. The tagged versions of PduB and PduJ were only found to interact with PduA. Thus it can be concluded that the majority of interactions within the outer shell of the microcompartment are mediated via PduA.

Gene Order Is Important for Organelle Biogenesis

In the natural *pdu* operon the first gene in the operon is characteristically *pduA*. In the artificial operon the order of the shell proteins was also kept largely the same, with *pduA* as the first gene in the sequence. To investigate the significance of this, a construct was made whereby the gene order was reversed in relation to the artificial operon that contains the minimal number of genes to allow for BMC formation. When this construct,

Table 1. Shell Protein Interactions

Bait Protein (His Tagged)	Prey PduA	PduB	PduJ	PduK	PduN	PduU	PduT	PduV	PduM
PduA	–	Y	Y	Y	Y	Y	N	N	N
PduB	Y	–	N	N	N	N	N	N	N
PduJ	Y	N	–	N	N	N	N	N	N
PduK	Y	N	N	–	N	N	Y	N	Y

A summary of protein-protein interactions occurring between shell proteins. Interacting proteins were initially determined by size on SDS-PAGE. Identity of bands was subsequently confirmed by MALDI. Bait protein is fused to an N-terminal His tag allowing purification by IMAC. Prey proteins contain no His tag. Y indicates positive interaction. N indicates a lack of interaction.

pduN-K-J-B-A, was transformed into *E. coli*, aberrant structures were observed that are similar to those seen when *pduA* was absent from the operon. Thus, the order of protein synthesis is important for correct organelle assembly, perhaps reflecting the importance of PduA in making many contacts with the other shell proteins during the construction of the BMC.

Targeting of Proteins to the Empty BMC

Although BMCs were formed with just PduA-B-J-K-N, they appeared slightly closer in terms of size and shape to those formed with the full operon when PduU was present. Therefore, for many of the further studies reported herein, the empty organelle was formed with a repertoire that also included PduU (i.e., PduA-B-J-K-N-U). In order to determine whether it is possible to direct a nonshell protein to the recombinant empty BMC, PduV was coproduced with the shell-forming complement (PduA-B-J-K-N-U). PduV is a protein of unknown function, although it does have some sequence similarity to members of the Ras-like GTPase superfamily. Indeed, purified PduV was found to have weak GTPase activity (data not shown). When PduV was coproduced with PduA-B-J-K-N-U, the protein was found to associate with the shell fraction of the cell lysate after purification by sucrose gradient ultracentrifugation (Figure 5A). This suggests that PduV may contain an internalization signal. To determine if PduV could be used as a vehicle for transport to the empty organelle, a GFP fusion was constructed. Thin sections of *E. coli* producing PduV-GFP were treated with an anti-GFP antibody and then with a secondary antibody conjugated to a 15 nm gold particle and compared to the staining observed with an *E. coli* strain producing both the PduV-GFP fusion and the PduA-B-J-K-N-U microcompartment. The results reveal that the gold particles were found only at the poles of cells producing the PduV-GFP fusion alone (Figure 5B), whereas in cells that contain both the PduV-GFP fusion and the PduA-B-J-K-N-U construct the gold particles were found largely associated with the microcompartments (Figure 5C). Thus, PduV can be used to direct protein to the BMC.

Protein targeting to the empty microcompartment was further explored by investigating the targeting of the two larger subunits of the diol dehydratase (PduC and PduD) using GFP in combination with live cell imaging. Control cells producing only the PduC-GFP construct gave an even distribution of cytoplasmic fluorescence, similar to that observed by the production of GFP alone (Figure 6). In contrast, both the PduD and PduV GFP fusion proteins produced fluorescence that was seen to localize largely at one pole of the cell, reflecting the insolubility of these proteins (Figure 6). However, when the PduC, PduD, and PduV GFP fusions were each coproduced with the recombinant BMC (PduA-B-J-K-N-U), fluorescent signals in the resulting strains were seen to be contained within discrete intracellular patches (Figure 6). When GFP was coproduced with the recombinant BMC, the fluorescence was dispersed throughout the cytoplasm and excluded from the microcompartments (Figure 6). In another control, using GFP fused to an unrelated non-Pdu protein, CbiG from *Methanothermobacter thermautotrophicus*, the GFP was located in patches at the poles of the cells that were producing the shell proteins and was not targeted to microcompartments (data not shown). These results are

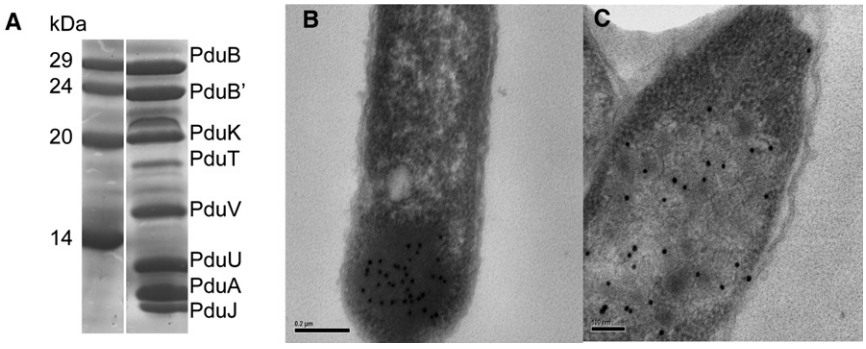

Figure 5. Incorporation of PduV into the Empty Bacterial Microcompartment

(A) SDS-PAGE of protein extract from strain expressing *pduA-B-J-K-N-U-T* and *pduV* after sucrose gradient ultracentrifugation (lane 2) in comparison to molecular mass standards (lane 1). The major bands in lane 2 were extracted, digested, and analyzed by MALDI to confirm their identity as shown. In comparison to Figure 2A, an extra band corresponding to PduV at around 16 kDa is observed.

(B) Thin section of an *E. coli* cell expressing the *pduV-GFP* fusion. A protein mass accumulates at one pole of the cell, and this area cross-reacts with anti-GFP antibodies and then with a secondary antibody conjugated to 15 nm gold particles.

(C) Thin section of an *E. coli* cell expressing both the shell protein complement (*pduA-B-J-K-N-U*) and the *pduV-GFP* fusion. Immunocytochemistry in this case reveals that the PduV-GFP fusion is located largely within the BMCs.

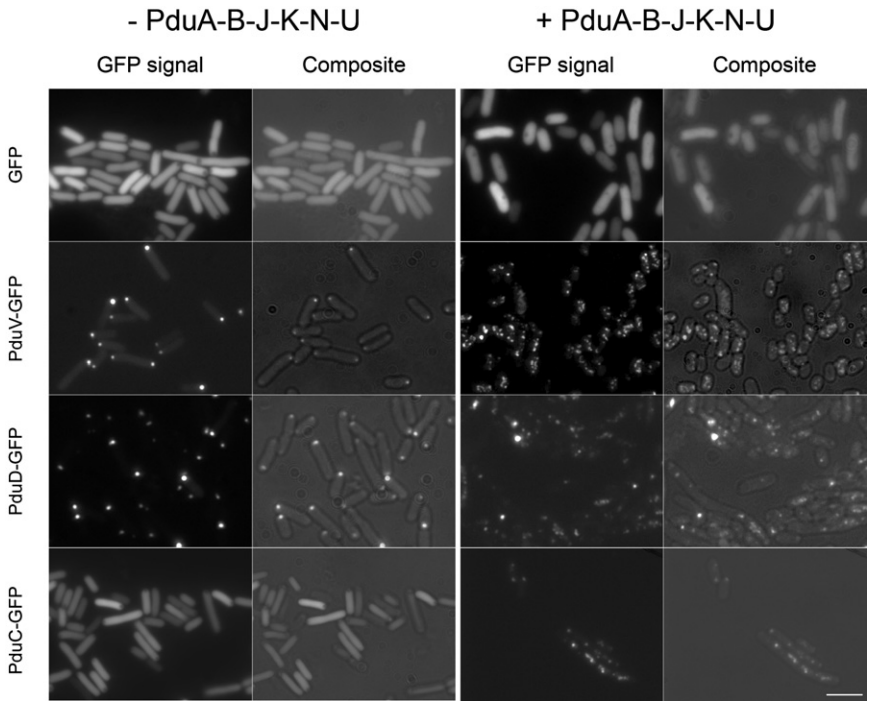

Figure 6. Cellular Distribution of PduC, PduD, and PduV Is Altered by the Presence of PduA-B-J-K-N-U Structures

E. coli cells were either transformed with a single plasmid expressing GFP, PduV-, PduC-, or PduD C-terminal GFP fusions or transformed with each of these plasmids in combination with the plasmid pLysS-pduABJKNU. GFP fluorescence from cells of each strain is presented in the left panels, with corresponding GFP phase composite images on the right. GFP alone localizes throughout the cytoplasm and is unaffected by the presence of the PduA-B-J-K-N-U complex. In contrast, while PduD and PduV localize to a discrete point at end of cells when expressed alone, coexpression of the PduA-B-J-K-N-U complex caused the PduV and -D to all associate with defined structures within the cytoplasm. While PduC-GFP alone has no discrete localization pattern, it recruits to the BMC when coproduced with PduA-B-J-K-N-U. Scale bar, 2 μm. See also Figure S2.

consistent with GFP being targeted to the BMCs when fused to proteins that are naturally located to the organelle.

N-Terminal Region of PduV Targets Protein to Organelle

To investigate which region of PduV is responsible for targeting to the organelle, the protein was truncated to give two variants that contain the first 42 and 98 amino acids of the original 151 amino acids of the protein, respectively. The truncated proteins were C-terminally fused with GFP to give PduV42-GFP and PduV98-GFP, and these were subsequently produced in *E. coli* with the shell proteins. Live cell imaging of *E. coli* cells producing PduV98-GFP revealed that 96% of cells have localized patches of GFP, consistent with the targeting of GFP to the microcompartments, although some patches of fluorescence are still observed at the poles of the cells (Figure S2). *E. coli* cells producing PduV42-GFP gave 87% of cells with localized patches of GFP throughout the cell, but more cells seem to have GFP located at the poles in comparison to cells producing full-length PduV-GFP (Figure S2). The fact that the fluorophore can still be incorporated into the microcompartments when PduV is shortened to only 42 amino acids indicates the N-terminal region is largely responsible for targeting to the microcompartments. To confirm this further, a variant of PduV missing the first 42 N-terminal amino acid residues was fused to GFP. When this construct was coproduced with the recombinant BMCs, only 9% of the fluorescence was directed to the organelles (data not shown). Thus, the N-terminal region of PduV plays an important role in directing the protein to the BMC, although contributions to the targeting must also come from the remainder of the protein, since the incorporation into the microcompartments is less efficient than that observed with the fuller-length versions.

Differential Localization of PduC, PduD, and PduV to the BMC

The localization of targeted proteins to the shell protein assemblies was further investigated by the synthesis of an mCherry variant of PduA. In this case, the gene for mCherry, a red fluorescent GFP variant, was cloned in-frame to the 5′ end of *pduA*. When the mCherry-PduA variant was coproduced with the other shell proteins (PduB-J-K-N-U), patches of red were observed throughout the cell (Figure 7A). Electron microscopy of thin sections of these cells indicated that the mCherry tag had little or no effect on microcompartment formation (data not shown). When GFP was produced with the mCherry-labeled BMC, no internalization was observed (Figure 7A). In contrast, when PduC-GFP, PduD-GFP, and PduV-GFP were individually coproduced with the mCherry-labeled BMC, red and green fluorescent signals coalesced at the same discrete structures (Figures 7B–7D). However, image analysis revealed that while PduC and -D were seen to localize within the interior of the microcompartments (Movie S3), PduV localized to cup-like structures upon the outer surface of the BMCs (Movie S4).

Protein Dynamics in the Macromolecular Assemblies

PduV-GFP was also observed to localize to elongated filaments, which frequently associated with the mCherry-PduA-labeled compartments (Figure 7D and Figure S3). Moreover, time-lapse analysis provides compelling evidence that there is some dynamic interplay between the mCherry-PduA-labeled patches when PduV-GFP is present (Movie S5). Indeed, these data suggest the PduV protein plays a role in regulating the spatial distribution of the microcompartments within the growing bacterial cell (Movie S5). In contrast, no movement is observed in equivalent cells expressing PduD-GFP (Movie S6).

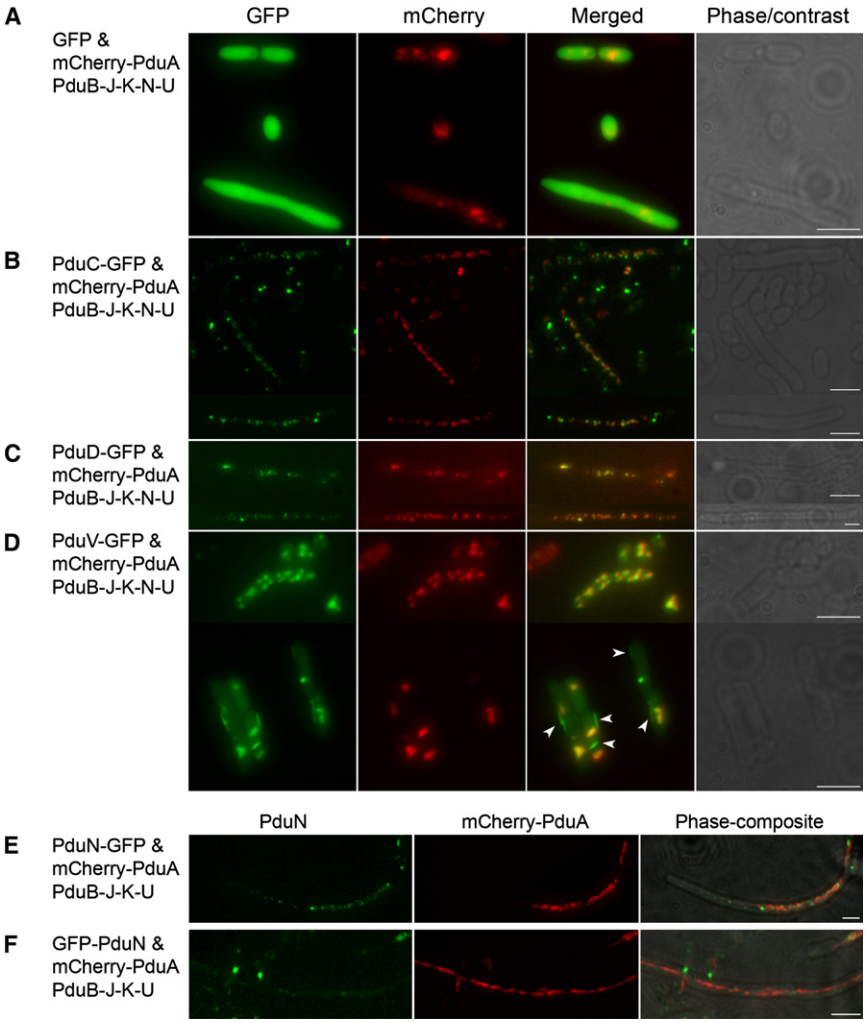

Figure 7. PduC, PduD, PduN, and PduV Are Recruited to PduA-B-J-K-N-U Structures

(A–D) GFP, mCherry, and merged GFP-mCherry fluorescence signals from *E. coli* cells containing pLysS*mCherry-pduA pduB-B′-J-K-N-U* in conjunction with plasmids containing cDNA encoding for either GFP alone (A) or GFP fused to the C-terminal of PduC (B), PduD (C), or PduV(D). PduC, PduD, and PduV GFP fusion proteins each colocalized with mCherry-labeled PduA-B-J-K-N-U structures, while GFP alone did not. PduV also localized to dynamic filaments (arrowheads), often seen associated the PduA-B-J-K-N-U structures (see also Figure S3 and Movie S6). Phase-contrast images (right column) show the cell outline.

(E and F) GFP, mCherry, and GFP-mCherry merged phase images of *E. coli* cells containing pLysS*mCherry-pduA pduB-B′-J-K-U* in conjunction with plasmids containing cDNA encoding for either C-terminal PduN-GFP (E) or N-terminal GFP-PduN fusion proteins (see also Figure S4 and). PduN-GFP localized to normal mCherry-labeled PduA-B-J-K-U structures. Scale bar, 2 μm.

Identification of PduN as a Component of the BMC

In an earlier section (above), it was demonstrated that the presence of PduN was required for the synthesis of the recombinant organelle, even though the recombinant protein has not been detected within the isolated superstructure (Havemann and Bobik, 2003) (Figure 3D). To investigate whether PduN could be detected associating with the organelle in vivo using GFP labeling, two GFP-labeled versions of PduN were constructed, where the fluorophore was fused to either the N or the C terminus of PduN. Consistent with EM studies, when mCherry-PduA was coproduced with the other core shell proteins except PduN (i.e., PduB-J-K-U), the microcompartments lost their spherical appearance and formed aberrant elongated filament-like structures that extended the longitudinal axis of the cell (Movie S7 and Figure S4). This BMC morphology defect was rescued by the coexpression of either PduN or a C-terminal PduN-GFP fusion protein (Movie S8 and Figure S4), the signal from which coincided precisely with that of the mCherry-PduA (Figure 7E). In contrast, the BMC structures remained elongated in identical cells producing the N-terminally tagged GFP-PduN fusion protein (Figure 7F), indicating the N terminus of PduN is crucial for its integration into the microcompartment structure.

DISCUSSION

In metabolism it is recognized that pathways and processes can be organized by the association of sequential enzymes into supramolecular complexes to allow for channeling and increased efficiency without the need for physical separation (Ovadi and Srere, 2000). Thus, the appearance of separate physical compartments, such as BMCs or organelles, has to be driven by a requirement for regions of the cell to have different physical properties (e.g., to allow the generation of gradients), different environments (e.g., to allow protein folding), or a necessity for barriers to allow the protection of the cell from potentially toxic compounds. Understanding how BMCs are assembled and organized not only provides important molecular detail on macromolecular assembly and localization but also provides insights into how compartmentalization can be designed for new or adapted biological functions.

To this end we have shown that the minimum complement of *pdu* metabolosome shell components required to form a microcompartment is six proteins (PduA-B-B′-J-K-N), compared with eight in the wild-type organelle. In the homologous carboxysome structure, it is predicted that between three and five shell proteins are required to encase the RuBisCO enzyme. The larger number of BMC-containing proteins required for metabolosome microcompartment formation may reflect the greater metabolic complexity of the structure, requiring it to facilitate a process demanding recycling of multiple cofactors, enzymatic reactivation, and channeling of multiple intermediary

metabolites. Out of these shell proteins the majority of interactions are mediated by PduA, as determined by protein-protein binding studies. This perhaps explains why PduA is the first encoded protein of the operon, allowing the newly synthesized protein to interact with the other shell components that are subsequently translated. Indeed, changing the order of gene expression prevents normal organelle formation, suggesting an important functional role for PduA in acting as a scaffold for the assembly.

The data presented here also reveal that PduN is crucial for BMC formation. As PduN bears similarity to CcmL, which forms a pentameric arrangement of subunits (Tanaka et al., 2008), it is possible that this protein forms the vertices of the microcompartment (Figure 1A). Only comparatively few vertices are required in icosahedral formation, and this may explain why PduN has not previously been detected either in the wild-type propanediol utilization metabolosome (Havemann and Bobik, 2003) or the recombinant structure specified by a complete *pdu* operon including *pduN* (Parsons et al., 2008). Live cell imaging has also confirmed the presence of PduN within the BMC. The fact that N-terminal tagging of PduN with GFP prevented BMC formation suggests that this region of the protein makes important contacts within the complex that are crucial for its structural integrity.

PduU and PduT are dispensable structural components of the microcompartment, as their absence does not prevent formation of the shell. PduU and PduT are therefore likely to have specialized roles within the metabolosome, perhaps in substrate/product permeation, or in the case of PduT, in a redox role, since this protein contains an Fe-S center. Significantly, we have recently shown that PduT interacts with PduS, a corrin reductase that also contains two 4Fe-4S centers (our unpublished data).

Of interest too is the appearance of large cytoplasmic axial filaments in *E. coli* by the overproduction of PduA alone. The appearance of ordered intracellular arrangements of filaments has been observed before in *E. coli*, mainly through the overproduction of bacterial actin homologs such as ParM (Salje et al., 2009). However, the overproduction of RNase E (CafA) not only produces similar axial filaments but also results in similar cellular morphological appearances in that septation is prevented during cell division (Carpousis, 2007; Nurmohamed et al., 2009; Okada et al., 1993; Okada et al., 1994). In vivo, RNase E together with other proteins such as enolase associated with the RNA degradosome are organized within the cell to form cytoskeletal-like helical structures (Carpousis, 2007; Nurmohamed et al., 2009). Interestingly, in *Salmonella enterica*, a tandem affinity purification and crosslinking method using PduB as bait showed association with enolase in vivo (Chowdhury et al., 2009).

The common link between these observations is a connection with the bacterial cytoskeleton. Indeed, in the presence of PduV the recombinant BMC appears to be associated with filaments. Shell protein interactions of this kind could enable positioning of the metabolosome in a particular zone of the cytoplasm. Live imaging of cells containing mCherry-PduA and PduV-GFP (together with PduB-J-K-N-U) indicates that movement of these proteins takes place within the cytoplasm, whereas if PduD-GFP replaces PduV-GFP, no movement is observed. Movement within the microcompartments therefore appears to be dependent upon the presence of PduV. As PduV is predicted to be a member of the Ras-like GTPase superfamily, it is tempting to speculate that PduV is, in some way, involved with cytoskeleton dynamics. It is interesting to note that the magnetosome, a lipid-bound organelle found in magnetotactic bacteria, is held in the cytoplasm by a network of cytoskeletal filaments (Komeili et al., 2006), and thus something similar may be happening with the BMCs.

Introducing compartmentalization into bacterial cells and targeting components to the compartment interior are important steps toward synthetic biology. Rather than having to revise or rewrite the genetic code to minimize or augment the global metabolic features of the host organism, targeting specific pathways to a microcompartment may simplify enhancement of cellular activity in the biosynthesis of nonnative metabolites, designer chemicals, vitamins, antibiotics, and biofuels. The rational design of specific bioreactors within a cell is likely therefore to have important biotechnological applications. The BMC meets all the criteria required of a nanoscale bioreactor: size, enzyme capture, and selective diffusion of substrate molecules and products, while retaining the catalytic species components and protecting them from degradation (Monnard, 2003). It has been shown that viral capsids can be used as such nanoreactors (Comellas-Aragones et al., 2007; Vriezema et al., 2005). There are several potential advantages of BMCs over a viral capsid for this function. First, they do not require an inactivation procedure to reduce infectivity, as viral nanostructures do (Rae et al., 2008). Second, the BMC has evolved for a primary metabolic function, as an enclosure for active metabolic enzymes (rather than viral nucleic acid and nucleases or lytic enzymes), and incorporates specific pores for the ingress of substrates and outward passage of reaction products.

Key to the success of any nanobioreactor is the ability to localize an enzyme within the structure. Toward this goal, we observe that proteins can be targeted to the BMC. By using PduC, PduD, or PduV as delivery vehicles, it is possible to localize GFP to the BMC. It appears that proteins can be differentially targeted to either the outside or the inside of the BMC. Live cell imaging revealed that both PduC and PduD are recruited to the interior of the organelle, whereas PduV locates to the outer surface and may then localize the structure to a specific region inside the cell. Targeting to the BMC is associated with the N-terminal sequence of the protein, since the tagging of GFP with the first 42 amino acids of PduV is enough to direct some of the protein to the organelle, whereas the absence of this motif leads to exclusion. The actual targeting sequences within all of the BMC-located proteins remain to be determined. Simple sequence alignments do not identify any recognized protein motifs. It has, however, been noted that the N-terminal regions of PduC-D-E, unnecessary for enzymatic function, exhibit a structurally similar pattern (hydrophobic residues followed by a less conserved potential linker region) to the unrelated C-terminal conserved sequence, which acts as a packaging signal for the 20 nm encapsulin bacterial nanocompartment (Sutter et al., 2008). It is likely that a candidate metabolosome targeting sequence will shortly be identified, and the combinatorial protein approach that we have applied to deduce structural principles will be utilizable to extend their metabolic repertoire.

EXPERIMENTAL PROCEDURES

Multiple Cloning of the Artificial *Citrobacter freundii pdu* Gene Constructs

Initially, the *C. freundii pdu* genes of interest encoding for organelle shell proteins (*pduABJKNU*) were cloned into the vector pET14b. Details of the various individual cloning procedures, together with a strain table of all the constructs used in this study, are given in the Supplemental Information.

TEM and Tomography

Thin sections of *E. coli* strains and transmission electron microscopy were undertaken as described previously (Parsons et al., 2008). Resin-embedded thin sections (~80 nm thick) of *E. coli* expressing PduA were imaged by electron tomography using standard methods as outlined in the Supplemental Information.

Antibody Production

Polyclonal rabbit antibodies, raised against the peptide RPHTDVEKILPKGISC corresponding to *C. freundii* PduA C-terminal residues 79–93 (gi|16760971), were obtained from New England Peptide (Gardner, MA, USA).

Immunogold Labeling

Standard procedures for immunogold labeling were employed for the detection and location of PduA and GFP and are described in detail in the Supplemental Information.

Live Cell Imaging of pduV-GFP and the Control Sample

Live cell imaging was undertaken as described previously (Skoumpla et al., 2007), with modifications as stated in the Supplemental Information.

Purification of Artificial Metabolosome Proteins

The artificial microcompartments and associated complexes were purified using the procedures described for the purification of the wild-type metabolosome using a combination of ultracentrifugation and sucrose density centrifugation. Further details are given in the Supplemental Information.

Pull-Down Assays and Protein Identification

Evidence of protein-protein interactions was determined by expressing various combinations in *E. coli*, one of which contained a His tag. Details are given in the Supplemental Information.

SUPPLEMENTAL INFORMATION

Supplemental Information includes four figures, one table, Supplemental Experimental Procedures, Supplemental References, and eight movies and can be found with this article at doi:10.1016/j.molcel.2010.04.008.

ACKNOWLEDGMENTS

We thank Dr. Ian Blomfield (Kent) for useful discussions on bacterial stress response and cell division, Dr. Beth Stroupe (Florida) for advice on electron microscopy, and Ian Brown for technical assistance. This work was supported by grants from the Biotechnology and Biological Sciences Research Council (BBSRC) and Science Foundation Ireland (SFI) to M.B.P. (06/RFP/GEN053). D.P.M. and M.J.W. are funded by BBSRC David Phillips and BBSRC Professorial fellowships, respectively.

Received: July 16, 2009
Revised: January 25, 2010
Accepted: April 2, 2010
Published: April 22, 2010

REFERENCES

Beeby, M., Bobik, T.A., and Yeates, T.O. (2009). Exploiting genomic patterns to discover new supramolecular protein assemblies. Protein Sci. *18*, 69–79.

Bobik, T.A., Havemann, G.D., Busch, R.J., Williams, D.S., and Aldrich, H.C. (1999). The propanediol utilization (pdu) operon of Salmonella enterica serovar Typhimurium LT2 includes genes necessary for formation of polyhedral organelles involved in coenzyme B(12)-dependent 1, 2-propanediol degradation. J. Bacteriol. *181*, 5967–5975.

Brinsmade, S.R., Paldon, T., and Escalante-Semerena, J.C. (2005). Minimal functions and physiological conditions required for growth of salmonella enterica on ethanolamine in the absence of the metabolosome. J. Bacteriol. *187*, 8039–8046.

Carpousis, A.J. (2007). The RNA degradosome of Escherichia coli: an mRNA-degrading machine assembled on RNase E. Annu. Rev. Microbiol. *61*, 71–87.

Cheng, S., Liu, Y., Crowley, C.S., Yeates, T.O., and Bobik, T.A. (2008). Bacterial microcompartments: their properties and paradoxes. Bioessays *30*, 1084–1095.

Chowdhury, S.M., Shi, L., Yoon, H., Ansong, C., Rommereim, L.M., Norbeck, A.D., Auberry, K.J., Moore, R.J., Adkins, J.N., Heffron, F., et al. (2009). A method for investigating protein-protein interactions related to Salmonella typhimurium pathogenesis. J. Proteome Res. *8*, 1504–1514.

Comellas-Aragones, M., Engelkamp, H., Claessen, V.I., Sommerdijk, N.A.J.M., Rowan, A.E., Christianen, P.C.M., Maan, J.C., Verduin, B.J.M., Cornelissen, J.J.L.M., and Nolte, R.J.M. (2007). A virus-based single-enzyme nanoreactor. Nat. Nanotechnol. *2*, 635–639.

Crowley, C.S., Sawaya, M.R., Bobik, T.A., and Yeates, T.O. (2008). Structure of the PduU shell protein from the Pdu microcompartment of Salmonella. Structure *16*, 1324–1332.

Havemann, G.D., and Bobik, T.A. (2003). Protein content of polyhedral organelles involved in coenzyme B12-dependent degradation of 1,2-propanediol in Salmonella enterica serovar Typhimurium LT2. J. Bacteriol. *185*, 5086–5095.

Iancu, C.V., Ding, H.J., Morris, D.M., Dias, D.P., Gonzales, A.D., Martino, A., and Jensen, G.J. (2007). The structure of isolated Synechococcus strain WH8102 carboxysomes as revealed by electron cryotomography. J. Mol. Biol. *372*, 764–773.

Kerfeld, C.A., Sawaya, M.R., Tanaka, S., Nguyen, C.V., Phillips, M., Beeby, M., and Yeates, T.O. (2005). Protein structures forming the shell of primitive bacterial organelles. Science *309*, 936–938.

Kofoid, E., Rappleye, C., Stojiljkovic, I., and Roth, J. (1999). The 17-gene ethanolamine (eut) operon of Salmonella typhimurium encodes five homologues of carboxysome shell proteins. J. Bacteriol. *181*, 5317–5329.

Komeili, A., Li, Z., Newman, D.K., and Jensen, G.J. (2006). Magnetosomes are cell membrane invaginations organized by the actin-like protein MamK. Science *311*, 242–245.

McGoldrick, H.M., Roessner, C.A., Raux, E., Lawrence, A.D., McLean, K.J., Munro, A.W., Santabarbara, S., Rigby, S.E., Heathcote, P., Scott, A.I., et al. (2005). Identification and characterization of a novel vitamin B12 (cobalamin) biosynthetic enzyme (CobZ) from Rhodobacter capsulatus, containing flavin, heme, and Fe-S cofactors. J. Biol. Chem. *280*, 1086–1094.

Monnard, P.A. (2003). Liposome-entrapped polymerases as models for microscale/nanoscale bioreactors. J. Membr. Biol. *191*, 87–97.

Nurmohamed, S., Vaidialingam, B., Callaghan, A.J., and Luisi, B.F. (2009). Crystal structure of Escherichia coli polynucleotide phosphorylase core bound to RNase E, RNA and manganese: implications for catalytic mechanism and RNA degradosome assembly. J. Mol. Biol. *389*, 17–33.

Okada, Y., Shibata, T., and Matsuhashi, M. (1993). Possible function of the cytoplasmic axial filaments in chromosomal segregation and cellular division of Escherichia coli. Sci. Prog. *77*, 253–264.

Okada, Y., Wachi, M., Hirata, A., Suzuki, K., Nagai, K., and Matsuhashi, M. (1994). Cytoplasmic axial filaments in Escherichia coli cells: possible function in the mechanism of chromosome segregation and cell division. J. Bacteriol. *176*, 917–922.

Ovadi, J., and Srere, P.A. (2000). Macromolecular compartmentation and channeling. Int. Rev. Cytol. *192*, 255–280.

Parsons, J.B., Dinesh, S.D., Deery, E., Leech, H.K., Brindley, A.A., Heldt, D., Frank, S., Smales, C.M., Lunsdorf, H., Rambach, A., et al. (2008). Biochemical

and structural insights into bacterial organelle form and biogenesis. J. Biol. Chem. *283*, 14366–14375.

Rae, C., Koudelka, K.J., Destito, G., Estrada, M.N., Gonzalez, M.J., and Manchester, M. (2008). Chemical addressability of ultraviolet-inactivated viral nanoparticles (VNPs). PLoS ONE *3*, e3315. 10.1371/journal.pone.0003315.

Rondon, M.R., Kazmierczak, R., and Escalante-Semerena, J.C. (1995). Glutathione is required for maximal transcription of the cobalamin biosynthetic and 1,2-propanediol utilization (cob/pdu) regulon and for the catabolism of ethanolamine, 1,2-propanediol, and propionate in Salmonella typhimurium LT2. J. Bacteriol. *177*, 5434–5439.

Salje, J., Zuber, B., and Lowe, J. (2009). Electron cryomicroscopy of E. coli reveals filament bundles involved in plasmid DNA segregation. Science *323*, 509–512.

Sampson, E.M., and Bobik, T.A. (2008). Microcompartments for B12-dependent 1,2-propanediol degradation provide protection from DNA and cellular damage by a reactive metabolic intermediate. J. Bacteriol. *190*, 2966–2971.

Schmid, M.F., Paredes, A.M., Khant, H.A., Soyer, F., Aldrich, H.C., Chiu, W., and Shively, J.M. (2006). Structure of Halothiobacillus neapolitanus carboxysomes by cryo-electron tomography. J. Mol. Biol. *364*, 526–535.

Skoumpla, K., Coulton, A.T., Lehman, W., Geeves, M.A., and Mulvihill, D.P. (2007). Acetylation regulates tropomyosin function in the fission yeast Schizosaccharomyces pombe. J. Cell Sci. *120*, 1635–1645.

Sutter, M., Boehringer, D., Gutmann, S., Gunther, S., Prangishvili, D., Loessner, M.J., Stetter, K.O., Weber-Ban, E., and Ban, N. (2008). Structural basis of enzyme encapsulation into a bacterial nanocompartment. Nat. Struct. Mol. Biol. *15*, 939–947.

Tanaka, S., Kerfeld, C.A., Sawaya, M.R., Cai, F., Heinhorst, S., Cannon, G.C., and Yeates, T.O. (2008). Atomic-level models of the bacterial carboxysome shell. Science *319*, 1083–1086.

Tanaka, S., Sawaya, M.R., and Yeates, T.O. (2010). Structure and mechanisms of a protein-based organelle in Escherichia coli. Science *327*, 81–84.

Vriezema, D.M., Aragones, M.C., Elemans, J.A.A.W., Cornelissen, J.J.L.M., Rowan, A.E., and Nolte, R.J.M. (2005). Self-assembled nanoreactors. Chem. Rev. *105*, 1445–1489.

Yeates, T.O., Kerfeld, C.A., Heinhorst, S., Cannon, G.C., and Shively, J.M. (2008). Protein-based organelles in bacteria: carboxysomes and related microcompartments. Nat. Rev. Microbiol. *6*, 681–691.